J Mol Model (2011) 17:1551–1563
DOI 10.1007/s00894-010-0849-7

ORIGINAL PAPER

Computational investigation of the histidine ammonia-lyase reaction: a modified loop conformation and the role of the zinc(II) ion

Amalia-Laura Seff · Sarolta Pilbák · Ioan Silaghi-Dumitrescu · László Poppe

Received: 27 May 2010 / Accepted: 2 September 2010 / Published online: 5 October 2010

Abstract Possible reaction intermediates of the histidine ammonia-lyase (HAL) reaction were investigated within the tightly closed active site of HAL from *Pseudomonas putida* (*Pp*HAL). The closed structure of *Pp*HAL was derived from the crystal structure of *Pp*HAL inhibited with L-cysteine, in which the 39–80 loop including the catalytically essential Tyr53 was replaced. This modified loop with closed conformation was modeled using the structure of phenylalanine ammonia-lyase from *Anabaena variabilis* (*Av*PAL) with a tightly closed active site as a template. Three hypothetical structures of the covalently bound intermediate in the *Pp*HAL active site were investigated by conformational analysis. The distances between the acidic *pro-S* β-hydrogen of the ligand and the appropriate oxygen atoms of Tyr53, Ty280 and Glu414 − which may act as enzymic bases − in the conformations of the three hypothetical intermediate structures were analyzed together with the substrate and product arrangements. The calculations indicated that the most plausible HAL reaction pathway involves the *N*-MIO intermediate structure in which the L-histidine substrate is covalently bound to the *N*-3,5-dihydro-5-methylidene-4*H*-imidazol-4-one (MIO) prosthetic group of the apoenzyme *via* the amino group. Density functional theory (DFT) calculations − on a truncated model of the *N*-MIO intermediate containing a Zn^{2+} ion coordinated to the imidazole ring of the ligand and to His83, Met382 and a water molecule − indicated that Zn-complex formation plays a role in the reactivity and substrate specificity of HAL.

Keywords Histidine ammonia-lyase · Loop conformation · Homology model · Conformational analysis · DFT calculation · Zn^{2+} ion

Abbreviations

$1GKM_{mod}$	Partially modified structure (in the 39–80 loop) of the histidine ammonia-lyase inhibited with L-cysteine (PDB code: 1GKM)
B3LYP	Becke's three parameter hybrid functional combined with the Lee-Yang-Parr correlation functional
CS	Systematic conformational search
DFT	Density functional theory
FC	Friedel-Crafts type mechanism
HAL	Histidine ammonia-lyase
MIO	3,5-Dihydro-5-methylidene-4*H*-imidazol-4-one
MM	Molecular mechanics force field
N-MIO	Covalent intermediate of the HAL reaction bound to MIO via the amino group of L-histidine
PAL	Phenylalanine ammonia-lyase
PAM	Phenylalanine 2,3-aminomutase
PDB	Brookhaven Protein Data Bank
TAL	Tyrosine ammonia-lyase
TAM	Tyrosine 2,3-aminomutase
QM	Quantum mechanics

Ioan Silaghi-Dumitrescu - deceased.

A.-L. Seff · I. Silaghi-Dumitrescu
Faculty of Chemistry and Chemical Engineering,
Babes-Bolyai University,
Cluj-Napoca 400028, Romania

S. Pilbák · L. Poppe (✉)
Department of Organic Chemistry and Technology
and Research Group for Alkaloid Chemistry,
Budapest University of Technology and Economics,
Budapest 1111, Hungary
e-mail: poppe@mail.bme.hu

Introduction

The degradation of histidine to glutamate follows a pathway different to that of other amino acids, whose degradation is catalyzed by transaminases [1]. In the first stage, histidine ammonia-lyase (HAL, EC 4.3.1.3) eliminates the α-amino group from L-histidine (L-His), yielding α,β-unsaturated (*E*)-urocanate (Fig. 1). (*E*)-urocanic acid is a component of human sweat and has been suggested to act as a sun blocker in human skin [2]. The absence of HAL in humans leads to a disease known as histidinemia [3].

HAL is a subset of the ammonia-lyase family along with phenylalanine ammonia-lyase (PAL, EC 4.3.1.24) and tyrosine ammonia-lyase (TAL, EC 4.3.1.23), which catalyze the deamination of the corresponding L-amino acids to (*E*)-cinnamic acid and (*E*)-coumaric acid, respectively [1]. *Pseudomonas putida* genes encode HAL (hutH) and *urocanase* (hutU) have been cloned and sequenced [4, 5]. HAL is also present in mammals (rat and human) [6–8]. An extensive analysis of the taxonomic distribution and phylogeny of PAL/TAL/HAL revealed that eukaryotic HAL, fungi PAL and the PAL of land plants have distinct origins [9]. The taxonomic distribution of HAL and PAL orthologues indicated that the ancestor of eukaryotes harbored HAL, while PAL was introduced by horizontal gene transfer in the ancestor of fungi and the ancestor of land plants [9]. HAL from *Pseudomonas putida* [10] was found to share 44, 43, 33, 32 and 31% amino acid sequence identity with *Rattus norvegicus* HAL [11], *Bacillus subtilis* HAL [12], *Anabaena variabilis* (bacterial) PAL [13], *Rhodosporidium toruloides* (yeast) PAL [14] and *Petroselinum crispum* (parsley) PAL [15], respectively.

The non-oxidative substrate deamination catalyzed by HAL, PAL and TAL requires the presence of a 3,5-dihydro-5-methylidene-4*H*-imidazol-4-one (MIO) electrophilic prosthetic group [16–18] in the enzyme. As indicated by a crystal structure study of three mutants (D145A, F329G and F329A) of HAL from *Pseudomonas putida* (*Pp*HAL) [19], MIO is formed autocatalytically by cyclization and dehydration of an Ala-Ser-Gly tripeptide (Fig. 2) [16, 19, 20]. The MIO prosthetic group was later identified in the crystal structures of yeast [14, 21], plant [15] and bacterial PAL [22] and bacterial TAL [23]. MIO was also identified in L-phenylalanine and L-tyrosine 2,3-aminomutases (PAM [24–26] and TAM [27, 28], respectively).

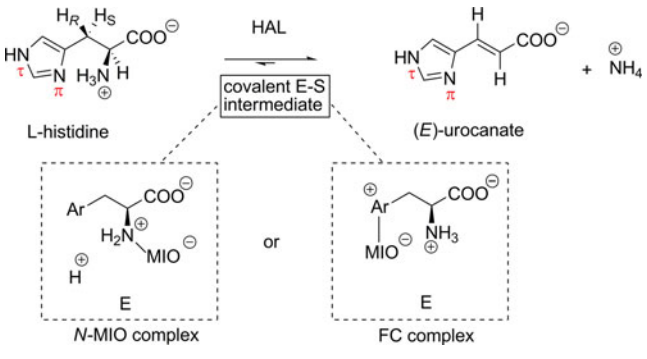

Fig. 1 The histidine ammonia-lyase (HAL) reaction with the proposed alternative reaction intermediates. Nitrogens in the imidazole rings of L-histidine and (*E*)-urocanate are denoted according to IUPAC with *pros* ("near", π) and *tele* ("far", τ)]

HAL, PAL and TAL should remove the non-acidic *pro-S* β-proton from their substrates without extracting the more acidic protons from the ammonium moiety of the corresponding L-amino acid [1]. Biochemical data have been interpreted by means of two significantly different mechanisms (Fig. 1) [1]. The first proposals for the mechanism of the ammonia elimination catalyzed by HAL [29] and PAL [30] suggested that an interaction between the amino group of the substrate and the electrophilic prosthetic group of the enzyme (i.e., an *N*-MIO intermediate) facilitates the reaction owing to the formation of a better leaving group [30, 31]. Due to the difficulty entailed by this possible mechanism in abstracting the non-acidic *pro-S* β-proton by the enzymic base during the course of ammonia elimination, an alternative mechanism involving a Friedel-Crafts (FC)-type attack at the aromatic ring of the substrates by the electrophilic prosthetic group was then suggested [32]. Despite the significant differences in the properties of these enzymes, the presence of similar electrophilic prosthetic groups seemed to indicate that HAL, PAL and TAL catalyze their respective reactions by analogous mechanisms [1].

Following elucidation of the structure of HAL by X-ray crystallography and the discovery of MIO (Fig. 2) [16], the importance of several amino acid residues at the active center (Tyr53, His83, Asn195, Gln277, Tyr280, Arg283, Phe329 and Glu414) for catalysis and substrate binding was evaluated by site-directed mutagenesis [33]. Mutagenesis was also performed for active site amino acid residues of PAL [34] that were identical or similar to the active site residues of HAL. The almost total loss of activity observed with mutant Y53F of HAL (2,650 times less active than wild-type HAL) and with mutant Y110F of PAL (75,000 times less active than wild-type PAL) demonstrated that Tyr53 in HAL and Tyr110 in PAL are essential for catalysis [33, 34].

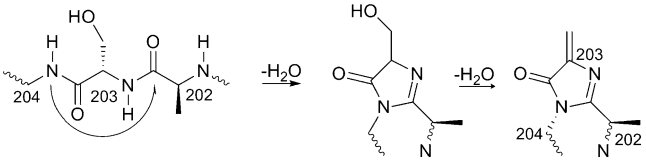

Fig. 2 Proposed autocatalytic formation of 3,5-dihydro-5-methylidene-4*H*-imidazol-4-one (MIO) from the tripeptide Ala-Ser-Gly

A unique feature of the reaction catalyzed by HAL is the significant enhancement of enzyme activity in the presence of divalent metal ions such as Zn^{2+}, Cd^{2+} or Mn^{2+} [35]. The optimal activity of HAL was shown to be dependent on the addition of metal ions [35, 36]. Based on these experimental data, it was proposed that the interaction of the substrate with the His83 imidazole group could be mediated by coordination with Zn^{2+} [33].

Although mutagenesis data [33] and six crystal structures [16, 19, 37] are available for HAL, the nature of the covalent reaction intermediate (Fig. 1) and the role of Zn^{2+} ion in catalysis have not been explored or investigated by systematic computations. It has been demonstrated already − in the case of the partially modified parsley phenylalanine ammonia-lyase (*Pc*PAL) − that homology modeling, systematic conformational search and ligand docking can be applied to mechanistic studies on an ammonia-lyase [34, 38, 39]. Based on the above data and methods, our goal in this study was to explore the structure of the covalent intermediate and the role of Zn^{2+} in the HAL reaction by using partial homology modeling, systematic conformational search and density functional theory (DFT) calculations.

Theory and methods

Experimental ammonia-lyase structures used for the computations

Six crystal structures of *Pseudomonas putida* histidine ammonia-lyase HAL were compared: {Brookhaven Protein Data Bank (PDB) codes: 1B8F, unliganded *Pp*HAL$_{Cys273Ala\text{-}mut}$ [16]; 1EB4, unliganded *Pp*HAL$_{Phe329Ala\text{-}mut}$ [19]; 1GK2, unliganded *Pp*HAL$_{Phe329Gly\text{-}mut}$ [19]; 1GK3, unliganded *Pp*HAL$_{Asp145Ala\text{-}mut}$ [19]; 1GKJ, unliganded *Pp*HAL$_{Tyr280Phe\text{-}mut}$ [37]; 1GKM, *Pp*HAL inhibited with L-cysteine [37]}. The six HAL structures exhibited only small differences in the positions of the amino acid side chains within the active center, with the exception of the arrangement of Met382 in the *Pp*HAL inhibited with L-cysteine (1GKM).

Modeling the Tyr53-containing 39–80 loop region of the *Pp*HAL structure

A HAL structure with a closed active site (1GKM$_{mod}$) was constructed by modifying the *Pp*HAL structure including the L-cysteine inhibitor (PDB code: 1GKM) by replacement of the 39–80 loop containing the catalytically essential Tyr53, in every subunit of the homotetrameric enzyme. The crystal structure of *Anabaena variabilis* phenylalanine ammonia-lyase PAL (PDB code: 3CZO) with a tightly closed active site [13] has been used as a template for modeling the closed conformation of the 39–80 loop of *Pp*HAL. For homology modeling, the SwissPDB Viewer [40–42] program suite and the Swiss-Model automated homology modeling service [43–46] were used.

Construction of covalently bound MIO–substrate intermediate models in the 1GKM$_{mod}$ structure

The L-cysteine inhibitor (Cys1510) within the modified structure of *Pp*HAL (1GKM$_{mod}$) was replaced by L-histidine. A portion of the 1GKM$_{mod}$ structure (overlapping spheres of 15 Å radius around the C_1 of the ligand and 12 Å radius around the O atom of the W544 water, consisting of 149 amino acid residues) was used as the active site model of *Pp*HAL for systematic conformational search (CS) calculations. For the CS analysis, three initial ligand structures [an *N*-MIO model and two diastereomeric (*S,S*)-FC and (*R,S*)-FC models] were built from this L-histidine by turning its carboxyl group towards Arg283 and its imidazole ring close to the HAL-specific His83 residue and constructing the appropriate bonds between the methylene carbon of MIO and the nitrogen atom of the amino group or C_4 atom of the imidazole of the ligand. Hydrogens were then added to the model portion of the 1GKM$_{mod}$ structures and the C- and N-termini at junctions were transformed into neutral aldehyde and amino moieties by HyperChem [47] standard procedure. The resulting structures were verified and corrected using Molfunction [48].

Conformational analysis of covalently bound MIO–substrate intermediates within the partial 1GKM$_{mod}$ structure

Two separate CSs were performed for each covalently bound reaction intermediate [*N*-MIO, (*S,S*)-FC and (*R,S*)-FC models] bearing a proton on either the π or the τ nitrogen of the imidazole ring (N_{π}H and N_{τ}H series of conformers). The six CS calculations involving the ligand and MIO [28 atoms in the *N*-MIO model and 29 atoms in the (*S,S*)-FC / (*R,S*)-FC models] were performed in a rigid enzymic environment without water molecules. For the *N*-MIO models, three torsions [along the axes of $C_{(MIO\text{-}C5)}$–$C_{(MIO\text{-}CH2)}$, $C_{(MIO\text{-}CH2)}$–$N_{(HisL)}$, $N_{(HisL)}$ – $C_{(HisL-C\alpha)}$], for the (*S,S*)-FC and (*R,S*)-FC models four torsions [along the axes of $C_{(MIO\text{-}C5)}$–$C_{(MIO\text{-}CH2)}$, $C_{(MIO\text{-}CH2)}$–$C_{(HisL\text{-}C4)}$, $C_{(HisL-C5)}$ – $C_{(HisL-C\beta)}$ and $C_{(HisL-C\beta)}$ – $C_{(HisL-C\alpha)}$] were varied, respectively, during CS. The CSs were performed using the HyperChem implemented CS module [47] with default settings (MM+ forcefield; gradient: 0.1 kcal mol^{-1}; Polak-Ribiere method; limits: 300 iterations, 150 optimizations, 15 conformations; test options: "skip if atoms are closer than 0.3 Å").

Geometry optimization of the covalent intermediates, L-histidine and (*E*)-urocanate within the active site of HAL

L-Histidine and (*E*)-urocanate structures were built − by appropriate rearrangement of bonds (Fig. 3) − only from conformers of the covalent intermediates with straight main-chain conformation [*N*-MIO series ($N_{\tau H}: c_1-c_3; c_5; c_8; c_9; c_{11}; N_{\pi H}: c_1 - c_4; c_6; c_9; c_{10}$); (*R,S*)-FC series ($N_{\tau H}: c_2; c_4; c_5; c_7 - c_9; N_{\pi H}: c_2$) and (*S,S*)-FC series ($N_{\tau H}: c_1 - c_2; N_{\pi H}: c_2$)]. In all substrate, intermediate and product structures, the ligand together with MIO (substrate, intermediate) or NH_2–MIO (product), and the His83, Tyr280, Tyr53, Asn195, Gln277, Glu414, Arg283 and Phe329 (a total of 116 atoms) were optimized in a 15 Å spherical region (2,221 atoms) of the $1GKM_{mod}$ structure while keeping the residual part rigid. The optimizations were performed using the HyperChem [47] implemented MM+ forcefield with default settings (gradient: 0.1 kcal mol^{-1}; Polak-Ribiere method).

Docking L-histidine and (*E*)-urocanate into the $1GKM_{mod}$ active site

The L-cysteine inhibitor and water molecules were removed from the $1GKM_{mod}$ structure, and a docking environment containing 29 amino acid residues (including His83, Arg283, Met382, Tyr53, Tyr280, Asn195 and Glu414 and MIO) was selected. For docking of the zwitterionic L-histidine, Tyr53 and Tyr280 were kept deprotonated and four torsion angles (along the axes of $C_5 - C_\beta$, $C_\beta - C_\alpha$, $C_\alpha - N$ and $C_\alpha - C_{COO}-$) were varied, whereas for docking of (*E*)-urocanate, protonated forms of Tyr53 and Tyr280 were used. Gasteiger charges were added to the atoms of the binding interfaces used for docking by AutoDock [49, 50]. During docking with AutoDock [49, 50], the zwitterionic L-histidine and (*E*)-urocanate were flexible in a rigid enzymic environment. The Grid Parameter File was established with default settings (Total Grid Pts per map: 77,326; number of points 40 for *x*- and *y*-dimensions, 45 for *z*-dimension; spacing: 0.375 Å; center on ligand) and docking processes were also run with the default settings (Lamarckian Genetic Algorithm: 10 runs; population size: 150; maximum number of energy evaluations: short setting).

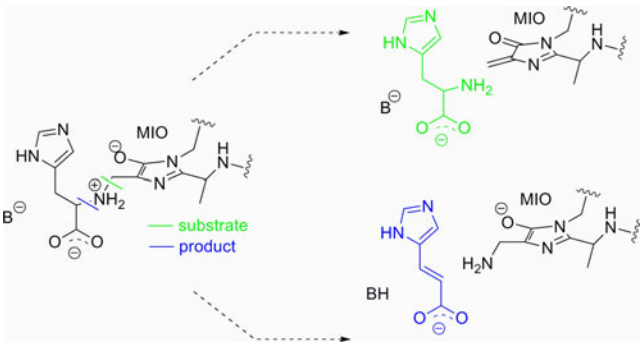

Fig. 3 Construction of the L-histidine (*green*)- and (*E*)-urocanate (*blue*)-containing active site models from the *N*-MIO intermediate model of HAL

DFT calculations on ligands involved in HAL reactions

DFT calculations were carried out on L-histidine and L-4-nitrohistidine models (both with protonated amino groups) for conformations corresponding to the HAL bound state, on a truncated model of the *N*-MIO-intermediate (by replacing the MIO ring of the calculated structure with a hydrogen atom at the exocyclic methylene carbon of MIO) and on a partial active site model including the truncated model of the *N*-MIO-intermediate in coordination with a Zn^{2+} ion, which is also coordinated to representative parts of His83 and Met382 and to a water molecule. The DFT optimizations were performed using GAUSSIAN 09 (rev. A.1) [51] and GaussView [52] as front-end. Two positively charged L-histidine structures (with –COOH and $-NH_3^+$) were constructed from the *N*-MIO models (from conformations c_5 and c_4 of the $N_{\tau H}$ and $N_{\pi H}$ series of CSs, respectively). Two positively charged L-nitrohistidine models were built from these two L-histidine structures by replacing the hydrogen at C_4 of the imidazole with a nitro group.

In the Zn^{2+} complex models, the Zn^{2+} ion had four or five ligands: the imidazole of the *N*-MIO ($N_{\pi H}$) ligand at the N_τ − atom (i.e., the c_4 conformer of the *N*-MIO $N_{\pi H}$ series, with a $-NH_2(CH_3)^+$ group as a model of the amino moiety bound to MIO, truncated between the MIO ring and the exocyclic carbon), a 4-methyl-1*H*-imidazole (coordinated at N_τ, representing His83), a dimethyl sulfide (coordinated at its S-atom, representing Met382) and one (in the tetrahedral case) or two (in the trigonal bipyramidal case) water molecules. Proper constraints were used to maintain the conformation of the MIO-bound histidine ligand (HisL) as allowed within the HAL active site. For the Zn^{2+} complex models, several atomic positions were frozen [in Model 1: an oxygen atom of carboxylic acid moiety of the MIO-bound histidine ligand (the one closer to Arg283), the carbon atom of the methyl group of 4-methylimidazole (truncated His83); in Model 2: as in Model 1+ a carbon atom of the dimethyl sulfide (representing the C_γ atom of Met382); in Model 3: as in Model 1 + methylene carbon atom of MIO; and in Model 4: as in Model 1+ a carbon atom of the dimethyl sulfide (representing the C_γ atom of Met382) and methylene carbon atom of MIO].

Full geometry optimizations for the two types of L-histidine, L-4-nitrohistidine and the tetrahedral or trigonal bipyramidal Zn^{2+} complexes were carried out by the DFT method using Becke's three parameter hybrid functional

combined with the Lee-Yang-Parr correlation functional (B3LYP) [53, 54], with the 6-31G or 6-31G(d,p) basis sets. After optimizations, vibrational frequencies were computed at the same level of theory and single point energies were calculated with a larger basis [6-311+G(d,p) for Zn^{2+}, for the two imidazole rings, for the –S-CH_3 part of Met382 and for the water molecule(s); and 6-31G(d) for the other parts of the Zn^{2+} complex models].

Results and discussion

Unfortunately, the available X-ray structures of HAL do not contain substrate, product or Zn^{2+} ion [16, 19, 37]. This may be due to the partially open active site of the available HAL structures (Fig. 4a). Therefore, the goals of this study were to generate an appropriate HAL enzymic environment in which to investigate the alternative enzyme-bound reaction intermediates and the role of Zn^{2+} ion by means of computation.

Construction of a closed HAL active site environment for calculations

For modeling the closed, active-site-containing state of HAL, the L-cysteine-inhibited *Pp*HAL [37] was selected as a starting structure (PDB code: 1GKM). This is the only crystal structure of *Pp*HAL in which an inhibitor is present. Importantly, this is also the structure where the side chain of Met382 has a different conformation from the side chain arrangement of the other five unliganded *Pp*HAL structures [16, 19].

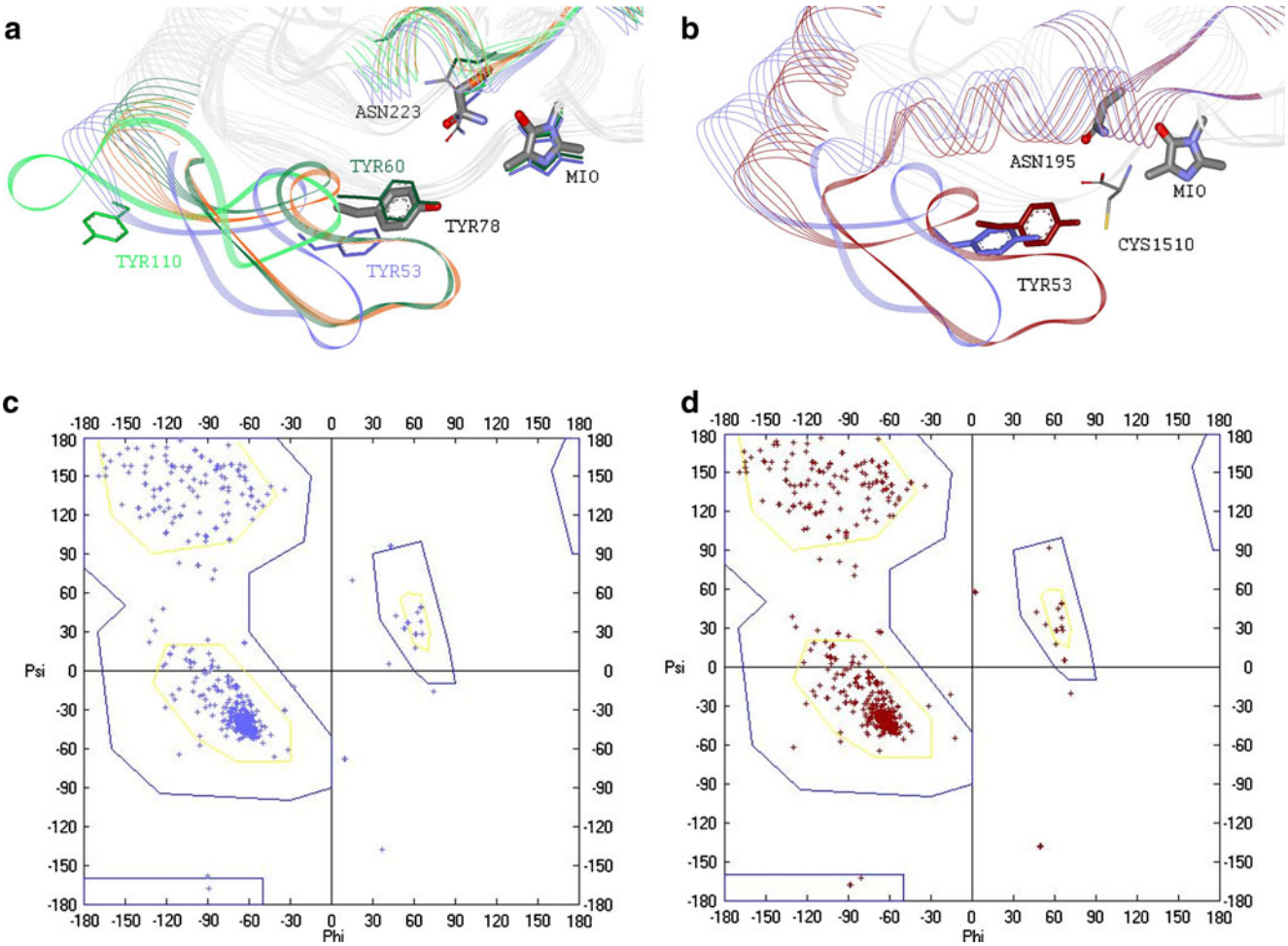

Fig. 4 Mobile Tyr-loops in the active site of MIO-containing ammonia-lyases. **a** Comparison of two mobile regions (including the MIO stabilizing Asn and the catalytically essential Tyr residues) of four different ammonia-lyases: *Anabaena variabilis* PAL [3CZO, in *orange* and *CPK* (Corey, Pauling, Koltun) color scheme]; *Petroselinum crispum* PAL (1W27, in *bright green*); *Rhodobacter sphaeroides* TAL (2O7B, in *dark green*); *Pseudomonas putida* HAL (1GKM, in *blue*). The Asn residue is numbered according to *Av*PAL (3CZO). **b** Overlay of essential Tyr53 loop regions of *Pp*HAL (1GKM inhibited with L-cysteine, colored in *CPK*, *blue chain*) and the Tyr-loop modified *Pp*HAL ($1GKM_{mod}$, *red chain*). **c**, **d** Ramachandran plots: **c** monomeric units of *Pp*HAL (1GKM), **d** partially modified *Pp*HAL ($1GKM_{mod}$)

Although the existing six *Pp*HAL structures contain Tyr53 in the active site [16, 19, 37], a structural comparison of HALs to other ammonia-lyases with tightly closed active sites indicated that the Tyr-loops in all HAL structures are in a partially open conformation (Fig. 4a). The importance of the loop containing the catalytically essential tyrosine in MIO-containing ammonia-lyases is best demonstrated for PAL. The Tyr-loops are missing [14, 21, 22] or in catalytically inactive conformation [15, 55] in several crystal structures of PAL. The active conformation of the Tyr-loop was confirmed only recently, in the structure of PAL from *Anabaena variabilis* (*Av*PAL) containing a tightly closed active site [13]. Similarly, the crystal structure of *Rhodobacter sphaeroides* tyrosine ammonia-lyase (*Rs*TAL) revealed a tight active center in which the loop containing the essential Tyr60 was present in the active conformation [23].

Comparison of the *Pp*HAL (1GKM, in blue) structure to *Rs*TAL (2O7B, in green) [23] and *Av*PAL (3CZO, in orange and CPK color) [13] with compact active centers revealed that the catalytically essential Tyr53-containing loop of *Pp*HAL adopts a partially open conformation (Fig. 4a). Because the most compact structure was found for *Av*PAL (3CZO, 2.2 Å resolution) containing the non-solvent accessible essential Tyr78 and the electrophilic MIO deeply buried in the active center [13], this ammonia-lyase structure was selected as a template for modeling the compact conformation of the Tyr-loop of *Pp*HAL.

Homology modeling successfully modeled the essential Tyr-containing loop region of PAL (*Pc*PAL, PDB code: 1W27 [15]), thus creating a proper active site environment for calculations inside PAL [38, 55]. Therefore, a similar strategy was used to construct the compact active site of *Pp*HAL. A partially modified *Pp*HAL crystal structure ($1GKM_{mod}$) was constructed by replacing the original 39–80 part (the partially open Tyr-loop) of every subunit of the L-cysteine inhibited *Pp*HAL crystal structure (1GKM) with a closed HAL Tyr-loop model based on the closed Tyr-loop conformation of the *Av*PAL structure [13].

Comparison of the Tyr53-containing inner loop region of the modified *Pp*HAL ($1GKM_{mod}$, Fig. 4b, in red) to the Tyr-loop of the original L-cysteine-inhibited *Pp*HAL (1GKM, Fig. 4b, in blue) indicated that the catalytically essential Tyr53 in the modified structure was closer to MIO, and therefore could better facilitate *pro-S* β-proton elimination from the substrate than the original HAL structure. Moreover, Ramachandran-plot analysis of single subunits of the two HAL structures revealed that there were eight amino acid residues outside the likely Phi/Psi combinations in the original HAL structure (1GKM, Fig. 4c), whereas there were only four unlikely combinations in the Tyr53-loop of the modified HAL structure ($1GKM_{mod}$, Fig. 4d).

Comparison of the conformation of covalent reaction intermediates of the HAL reaction with the arrangements of the substrate and product

Some early reports had indicated that treatment of HAL at high pH in the presence of L-cysteine and oxygen leads to an irreversible inactivation of the enzyme [56, 57]. Upon denaturation, followed by pronase digestion, the L-cysteine-inhibited HAL, results in two main chromophoric products [58]. In one product, the exocyclic methylene of the MIO was substituted by the amino groups of L-cysteine. When L-cysteine-inhibited HAL was first digested with trypsin, two chromophoric 24-residue peptides were isolated and identified as *N*-MIO fragments [59]. This was later supported by the L-cysteine inhibited structure of *Pp*HAL (PDB code: 1GKM) [37]. The inhibited HAL contains the inhibitor with its amino moiety close to the exocyclic methylene of the electrophilic MIO prosthetic group. This fact can be considered as a further proof of the presence of an amino-enzyme intermediate in the HAL reaction, as demonstrated by Peterkofsky [60].

Structures of HAL with L-cysteine [37], TAL with 2-aminoindan-2-phosphonate inhibitor [23] and TAM co-crystallized with α,α-difluoro-β-tyrosine [61] or *p*-fluorocinnamate epoxide [62] provided strong evidence for reactions via *N*-MIO intermediates (in which the substrate is connected to MIO through its amino group) for the ammonia-lyase and aminomutase reactions. An alternative covalently bound intermediate was proposed by Rétey and coworkers [32]. In this case, a σ-complex would be formed between the aromatic part of the substrate and the MIO prosthetic group by an FC-like mechanism.

Analysis of the active site residues surrounding the ligand in the L-cysteine-inhibited HAL [37] indicated that the *pro-S* β-proton from the L-histidine substrate can be abstracted by one of the three residues (Tyr53, Tyr280, Glu414) that might be considered as enzymatic bases (Fig. 5). Mutagenesis experiments also demonstrated that Tyr53, Glu414 [33], and Tyr280 [33, 37] are important residues for catalysis. The remarkably reduced catalytic activity of the analogous tyrosine (Tyr60 and Tyr300) mutants of TAL [63] underlines the importance of Tyr53 and Tyr280 in the HAL reaction.

Investigation of PAL with the phenylalanine analogues D- and L-2-aminooxy-3-phenylpropionic acid deduced that ammonia elimination approximates the course of least-motion [64]. In several *Rs*TAL structures, products of the elimination reaction were found in the active site in a zig-zag orientation [23]. The least-motion course principle and the similar straight chain zig-zag shape of the (*E*)-urocanate product of the HAL reaction determine a straight chain zig-zag arrangement of the covalently bound intermediate and also the L-histidine substrate. Irrespective of the nature of the covalently bound reaction intermediate, four reaction paths can fulfill these requirements (Fig. 5).

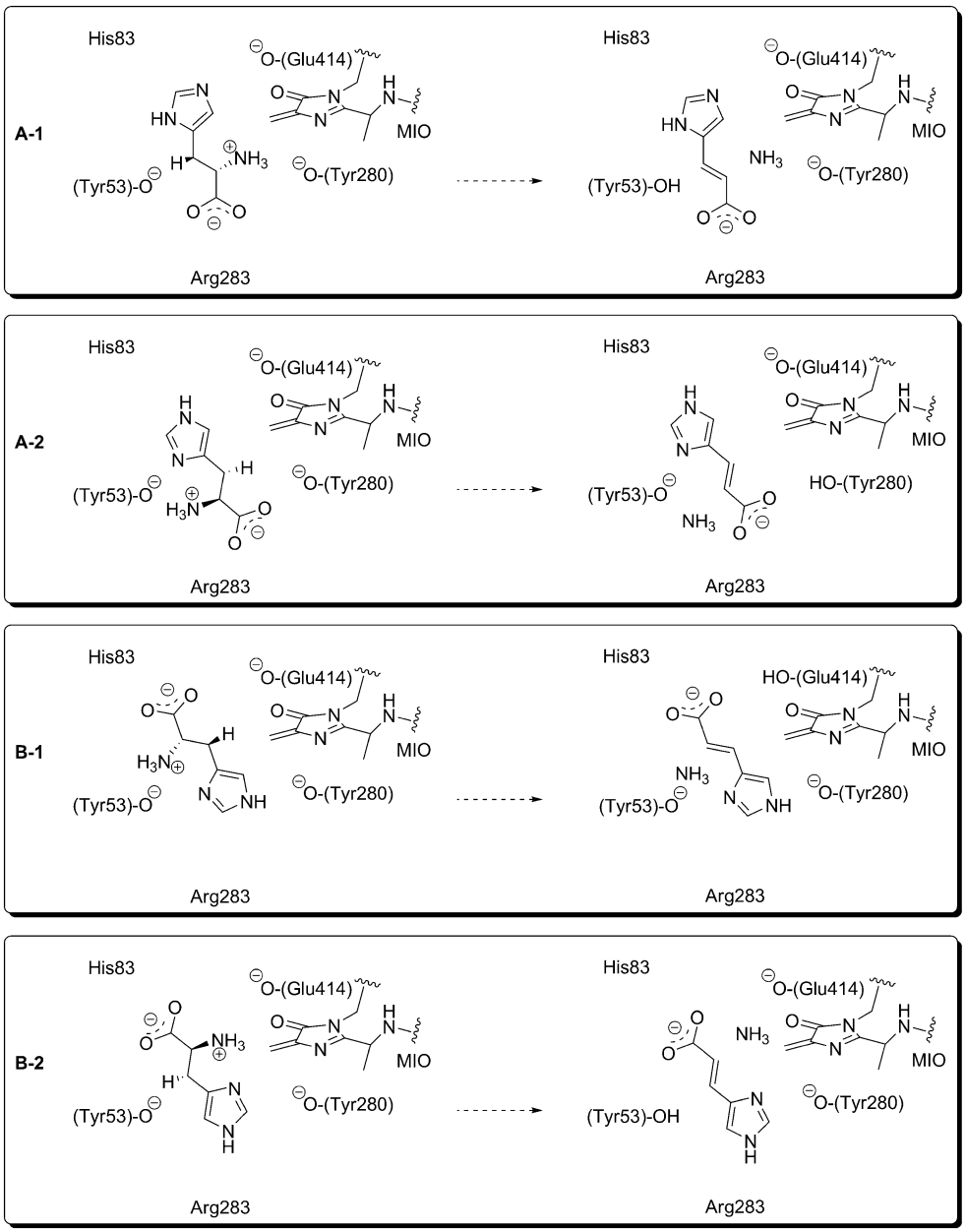

Fig. 5 Four possible arrangements of L-histidine and (*E*)-urocanate along the reaction pathways (*A-1*, *A-2*, *B-1* and *B-2*) assuming the course of least-motion in the HAL active site containing the MIO prosthetic group, His83, Arg283 and three possible enzymatic bases: Tyr53, Tyr280 and Glu414

Along the **A-1** reaction path for transformation of the substrate to product, both *N*-MIO and FC intermediates are possible, but only the Tyr53 amino acid could abstract the *pro-S* β-proton from the substrate. Only an FC-like mechanism is possible via the **A-2** path involving Tyr280 as the base for *pro-S* β-proton abstraction. Along the **B-1** path, deamination of L-histidine may take place by the FC mechanism involving Glu414 as an enzymic base. Along the **B-2** path, both types of mechanism (*N*-MIO and FC) can be taken into account, involving Tyr53 as the base for abstraction of the *pro-S* β-proton.

In addition to the substrate and product states (Fig. 5), the covalently bound reaction intermediate should also fulfill the requirements of least-motion course in the HAL active site. If the HAL reaction proceeded via the *N*-MIO intermediate, the amino moiety of the L-histidine substrate would be bound to MIO. If the HAL reaction proceeded via an FC-type intermediate, the C_4 carbon of the aromatic ring of L-histidine substrate would form a σ-complex with MIO. However, in this case the reaction may take place via two diastereomeric intermediates [(*S,S*)-FC and (*R,S*)-FC] due to a newly forming center of asymmetry at the C_4 carbon of the aromatic ring in the σ-complex.

As the substrate was anchored to the enzyme by a covalent bond in all cases of possible intermediates, systematic CS with the alternative reaction intermediates was a powerful tool with which to find possible arrangements within the HAL active site. Because none of the six

HAL [16, 19, 37] crystal structures indicated significant variation within most of the active center, the CSs were performed in rigid enzyme environment. This approach was also supported by the analysis of the B-factors of the active site amino acid residues, which indicated low mobility (with the exception of the residues of the mobile Tyr53-loop).

Because the imidazole ring allowed two different protonation states ($N_{\tau H}$ or $N_{\pi H}$) for each reaction intermediates, six CSs were performed for the three principal alternatives [$N-\mathrm{MIO}-N_{\tau H}$, $N-\mathrm{MIO}-N_{\pi H}$, $(R,S)-\mathrm{FC}-N_{\tau H}$, $(R,S)-\mathrm{FC}-N_{\pi H}$, $(S,S)-\mathrm{FC}-N_{\tau H}$, $(S,S)-\mathrm{FC}-N_{\pi H}$]. Only those conformations that had a straight chain zig-zag arrangement within the lowest 10 kcal mol^{-1} range were kept (Table 1). From the retained conformations of the covalent intermediates of the six CSs, L-histidine- and (*E*)-urocanate-containing active site models were con-

Table 1 Molecular mechanics force field (MM) relative energies of the models of substrate (E_S), intermediate (E_I) and product with 3,5-dihydro-5-methylidene-4*H*-imidazol-4-one (MIO)-bound amino group (E_{P+NH2}) and representative H–O distances in the covalent substrate–MIO intermediate structures

Covalent intermediate [a]	Relative energies [b] (kcal/mol)			Reaction path [c]	H-O distances (Å) in I [d]			
	E_S	E_I	E_{P+NH2}		R283	Y53	Y280	E414
N-MIO ($N_{\tau H}$)								
c_1	14.0	7.8	-10.1	A-1	**2.19**/3.12	**2.31**	5.17	6.14
c_2	5.6	2.7	-7.5	A-1	3.73/5.20	**2.29**	5.09	5.43
c_3	14.0	8.3	-10.7	A-1	**2.19**/3.03	**2.33**	5.23	6.50
c_5	13.9	0.2	-10.0	A-1	**2.28**/3.08	**2.36**	5.21	6.45
c_8	5.7	0.0	-10.7	A-1	4.37/6.09	**2.37**	5.30	5.64
c_9	14.7	7.8	-5.4	B-2	8.41/7.45	**2.13**	4.25	4.83
c_{11}	21.8	15.4	-5.8	A-1	**2.36**/2.89	**2.15**	5.13	6.20
N-MIO ($N_{\pi H}$)								
c_1	20.4	11.3	14.9	A-1	4.08/5.36	**2.45**	5.04	5.28
c_2	40.4	10.8	0.4	A-1	3.74/5.20	**2.34**	5.12	5.44
c_3	24.1	17.9	8.5	A-1	**2.18**/3.12	**2.28**	5.16	6.14
c_4	24.0	17.6	6.2	A-1	**2.19**/3.03	**2.31**	5.15	6.24
c_6	24.2	19.7	5.5	A-1	**2.19**/2.69	**2.44**	5.12	6.28
c_9	31.7	24.1	8.2	A-1	**2.32**/2.85	**2.22**	5.15	6.19
c_{10}	24.9	16.5	5.1	B-2	7.68/8.63	**2.15**	4.13	4.75
(*R*,*S*)-FC ($N_{\tau H}$)								
c_2	30.5	23.1	13.4	B-2	7.64/8.24	4.23	5.40	4.96
c_4	28.7	24.0	10.9	B-1	8.79/9.09	4.14	5.43	5.42
c_5	26.3	23.1	11.7	B-1	8.24/7.64	4.15	5.39	5.15
c_7	28.7	27.2	15.7	B-1	7.41/7.89	2.66	3.18	4.02
c_8	25.0	33.1	15.4	B-1	7.97/8.60	4.07	2.63	2.70
c_9	28.8	25.9	11.8	B-1	8.99/9.01	3.45	5.84	6.53
(*R*,*S*)-FC ($N_{\pi H}$)								
c_2	25.5	22.8	10.5	B-1	7.63/8.22	4.80	3.71	2.59
(*S*,*S*)-FC ($N_{\tau H}$)								
c_1	27.9	28.6	3.2	B-1	7.34/7.90	2.67	2.92	4.15
c_2	25.3	29.0	2.9	B-1	7.87/8.12	2.60	3.00	4.21
(*S*,*S*)-FC ($N_{\pi H}$)								
c_2	27.8	28.5	6.8	B-1	7.53/8.11	2.63	2.92	4.21

[a] The c_1–c_n notations refer to the covalent intermediate conformations obtained by calculations described in the section Conformational analysis of covalently bound MIO–substrate intermediates within the $1GKM_{mod}$ structure

[b] The methods for optimization of the substrate (S), intermediate (I) and product ($P+NH_2$) states are described in the section Geometry optimization of the covalent intermediates, L-histidine and (*E*)-urocanate within the active site of HAL

[c] The types of arrangements (according to Fig. 5) are shown only for those S → I → P(+NH_2) reaction pathways that satisfy the least-motion principle

[d] Distances between the carboxylate-O of the ligand and the two N-H groups of Arg283, and between the *pro-S* β-hydrogen of the intermediate (I) and the O^- atoms of the possible enzymatic bases Tyr53/Tyr280/Glu414. Distances shorter than 2.5 Å are shown in *bold*

structed. The substrate and product and the surrounding eight catalytically relevant amino acid residues were optimized within the closed HAL ($1GKM_{mod}$) active site. In this way, comparative analysis of the full S → I → P(+NH_2) reaction pathways become feasible (Table 1).

Although energies obtained at the MM level of theory are usually not accurate enough for reliable enzyme mechanistic studies, several observations are worth mentioning. According to our calculations (Table 1), energetic results also favor the reaction via *N*-MIO ($N_{\tau H}$) type intermediates (especially via the c_5 and c_8 conformations). In the *N*-MIO ($N_{\tau H}$) case, the substrate binding states are of substantially higher energy than the corresponding reactive *N*-MIO type intermediates, and the product binding states are of the lowest energies. As the energy of the substrate biding state is substantially higher than the energy of the corresponding product binding state in all cases of the *N*-MIO ($N_{\tau H}$) type route, the calculated energy profile of the reaction is in full agreement with experimental results since MIO-containing ammonia-lyases catalyze, under normal conditions, ammonia elimination from the L-amino acids in a practically irreversible manner [1, 18]. Although other types of intermediates can be disclosed as reactive species by non-energetic arguments discussed later, it is worth noting that all the other intermediate structures had higher energies (10.8–33.1 kcal mol^{-1}) than the lowest energy *N*-MIO ($N_{\tau H}$) intermediate conformer.

Next, the H–O distances in the optimized structures of the MIO-bound intermediate models between the *pro-S* β-hydrogen of the ligand and the oxygen atoms of the possible enzymic bases (Tyr53, Tyr280 and Glu414) and between the carboxylate oxygen group of the ligand and Arg283 were analyzed (Table 1). The most decisive result of this analysis was the observation that no enzymic base in any of the FC-intermediate conformations was close enough to the *pro-S* β-hydrogen to abstract it. Therefore, the **A-1** pathway involving an *N*-MIO covalent intermediate is the most plausible for the HAL reaction, but a **B-2** type orientation would also be allowed.

The optimized structures containing L-histidine and (*E*)-urocanate ligands in the active site of the closed HAL structure were compared to the arrangements of these ligands obtained by a docking procedure. Analysis of the AutoDock results revealed a well conserved orientation of the product (the carboxylate of the ligand is in the vicinity of the Arg283 while the imidazole moiety points towards His83) and agreed with the results obtained from the MM optimizations. Taking into account the orientation of the product within the active site, the docking results corresponded only to the **A-1** pathway.

The role of Zn(II) in the HAL reaction

The first known zinc-containing enzyme, carbonic anhydrase, was discovered in 1932 and was found to contain bound zinc associated with catalytic activity [65, 66]. Nowadays, many enzymes are known to contain zinc coordinated to two or three histidine residues and to other residues or water molecules [67–69]. Enzymes may contain two histidines both coordinating the Zn ion by their N_π atoms [70, 71] or at their N_τ atoms [72], or in some cases the Zn ion is coordinated by one His at N_π, and by the other His at N_τ [70, 72–74].

It was observed that Zn^{2+} or a number of different divalent cations, such as Cd^{2+} or Mn^{2+}, increase the activity of HAL [35]. On the other hand, there is no Zn^{2+}-containing crystal structure for HAL [16, 19, 37]. This apparent contradiction can be resolved by assuming that Zn^{2+}, which is necessary for catalytic activity, interacts during the HAL reaction with the HAL-specific His83 residue and with the imidazole of the substrate [33]. Therefore, the reason why no Zn^{2+}-containing HAL structure is known is that no substrate- or product-containing HAL structure has been determined so far [16, 19, 37]. Interaction of a Zn^{2+} with the HAL-specific His83 and with the substrate during catalysis [33] could also rationalize why HAL accepts only L-histidine [1], L-4-fluorohistidine [75] or L-4-nitrohistidine [32, 76] as substrates.

To examine the contribution of Zn^{2+} to HAL reaction, model studies were performed on the conformations found for the *N*-MIO intermediate in the $1GKM_{mod}$ active site. Analysis of the existing Zn-containing protein crystal structures [70–74] and the calculated *N*-MIO intermediate conformations led to the conclusion that Zn could be coordinated at N_τ atoms of His83 and of the imidazole group of the substrate (Fig. 6a), as was found in Adamalysin II, a zinc endopeptidase from the snake venom of *Crotalus adamanteus* [77] (Fig. 6b).

Two kinds of Zn-complexes can be found in Zn-containing protein structures [73, 74]. The Zn may be present in tetrahedral (Th) [73, 74] or trigonal bypiramidal (Tbp) [70, 71] complexes. During the HAL reaction, the further ligands of the Zn^{2+} coordinated to His83 and to the imidazole of L-histidine could be the S atom of the Met382 − a residue conserved in histidine ammonia-lyases − and one (in a tetrahedral Zn-coordination, Th) or two water molecules (in a trigonal bipyramidal Zn-coordination, Tbp).

DFT calculations were performed on the two kinds of truncated Zn-complex structures (Th and Tbp) including all important parts of the active site of HAL (partial elements of MIO, His83, Met382 and one or two conserved water molecules). The DFT calculations indicated that the reaction of HAL should include a tetrahedral Zn-complex, because only tetrahedral complexes resulted in reasonable structures (Table 2). Optimizations of all possible kinds of trigonal bipyramidal Zn-complex arrangements aborted or led to tetrahedral structures by exclusion of a water. Comparison of the tetrahedral Zn-complex (Fig. 6c) with the Zn^{2+} complex found in Adamalysin II [77] (Fig. 6b) and with the possible arrangement of the substrate–MIO

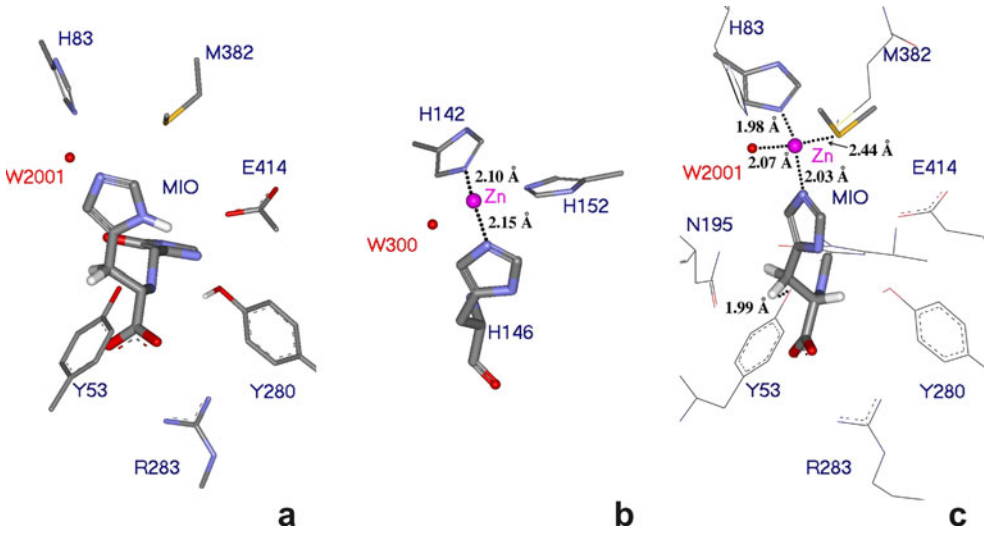

Fig. 6 **a** Arrangement of the covalent *N*-MIO intermediate ($N_{\pi H} - c_4$) in the active site of HAL (1GKM$_{mod}$). **b** The tetrahedral coordination of Zn (in *pink*) in the Adamalysin II, a zinc endopeptidase from the snake venom of *Crotalus adamanteus* [77] (PDB code: 1IAG). **c** Fit of the tetrahedral Zn-complex model (Model 4, by DFT calculation) into the ligand-free active site of HAL (1GKM$_{mod}$)

covalent intermediate obtained by conformational analysis in the Zn-free active site (Fig. 6a) indicated good agreement in the spatial arrangement of the structures.

The overlay of the truncated tetrahedral Zn-complex and the ligand-free HAL structure (Fig. 6c) indicated that N_τ atom of the ligand imidazole was involved in the Zn coordination, whereas the hydrogen atom on the N_π position could be at H-bond distance from Glu414 (Fig. 6a,c). The binding of the ligand during the HAL reaction at its imidazole ring by His83 via the Zn-complex and by Glu414 via a hydrogen bond is in full agreement with active site mutation data, indicating that the Glu414Ala ($k_{cat}/k_{cat\text{-}mut}$=20,930) and the His83Leu ($k_{cat}/k_{cat\text{-}mut}$=18,000) mutations have the most dramatic effect on catalysis [33]. Although other mechanisms of zinc(II) activation of the enzyme can be considered, this mode of substrate binding can rationalize the very narrow substrate specificity (in addition to L-histidine, only L-4-fluorohistidine [75] and L-4-nitrohistidine [32, 76] are accepted as substrates [1]) of HAL as well.

All the previous results implied that the enzymic base in the HAL reaction which abstracts the *pro-S* β-hydrogen as a proton is Tyr53. This was also indicated by the 1.99 Å distance between the oxygen atom of Tyr53 and the *pro-S* β-hydrogen of the tetrahedral Zn-complex (Fig. 6c).

Although Mulliken charges cannot be used as clear arguments for the acidity of hydrogen atoms, analysis of Mulliken charges of the *pro-S* β-hydrogens of L-histidine, L-4-nitrohistidine and truncated models for the Zn-free and Zn-coordinating *N*-MIO intermediates in the conformations allowed in the closed active site of HAL was performed (Table 3). L-4-Nitrohistidine was also included because it is known that the nitro group acidifies the *pro-S* β-hydrogen of L-4-nitrohistidine [76], and it is accepted as a substrate even by the MIO-less mutant of HAL [32]. The Mulliken

Table 2 Bond lengths and energies for tetrahedral zinc-ligand complex models calculated by density functional theory (DFT) methods

Model	Relative energies (kcal/mol)[a]	Distances (Å)[b]			
		Zn-N$_{His83}$	Zn-N$_{HisL}$	Zn-O$_{HOH}$	Zn-S$_{Met382}$
1	1.00(0.44)	1.97(1.96)	2.02(2.01)	2.07(2.05)	2.42(2.50)
2	0.00(0.00)	1.96(1.96)	2.03(2.01)	2.06(2.05)	2.42(2.51)
3	2.32(1.57)	1.96(1.96)	2.02(2.01)	2.08(2.05)	2.41(2.49)
4	1.84(0.19)	1.98(1.96)	2.03(2.02)	2.07(2.05)	2.44(2.51)

[a] By single point calculation at QM/QM B3LYP/6-311+G(d,p):B3LYP/6-31G(d) level after optimization of the structures at B3LYP/6-31G(d,p) level; values in brackets are from single point calculations at QM/QM B3LYP/6-311+G(d,p):B3LYP/6-31G(d) level after optimization of the structures at B3LYP/6-31G level

[b] Bond lengths in Zn-complexes optimized at B3LYP/6-31G(d,p) level; values in brackets are for Zn-complexes optimized at B3LYP/6-31G level

Table 3 Mulliken atomic charges of the *pro-S* β-hydrogens in zwitterionic L-histidine, in zwitterionic L-4-nitrohistidine, in a truncated *N*-MIO-intermediate model and in the tetrahedral Zn-complex models

Entry	Structure[a]	H_S	H_R
1	N-MIO (truncated model)	0.176 (0.221)	0.133 (0.173)
2	L-Histidine	0.180 (0.222)	0.102 (0.166)
3	L-4-Nitrohistidine	0.199 (0.245)	0.135 (0.201)
4	Zn-complex, Model 1	0.220 (0.267)	0.172 (0.206)
5	Zn-complex, Model 2	0.220 (0.265)	0.173 (0.208)
6	Zn-complex, Model 3	0.220 (0.263)	0.174 (0.208)
7	Zn-complex, Model 4	0.215 (0.261)	0.177 (0.210)

[a] Calculations on the ligand conformations allowed within the HAL active site were performed at B3LYP/6-31G(d,p) level (values in brackets are from B3LYP/6-31G DFT calculations)

charges found for *pro-S* β-hydrogen at the optimized geometries of L-histidine, L-4-nitrohistidine ($N_{\tau H}$ forms) and the Zn-complex models (Table 3) indicated that the *pro-S* β-hydrogen was significantly more polarized in L-4-nitrohistidine (Entry 3) than in the L-histidine (Entry 2) or in the Zn-free *N*-MIO model (Entry 1). The most charged *pro-S* β-hydrogens, however, were found in the Zn-complex models (Entries 4–7).

These results imply that the formation of a transient Zn-complex in the HAL reaction contributes not only to the specific binding of the substrate but to the enhancement of its reactivity as well. Further details of the HAL reaction and the Zn-complex will be studied on a QM/MM model of the full active site of HAL in the near future.

Conclusions

The present study revealed that the existing experimental structures of histidine ammonia-lyase from *Pseudomonas putida* (*Pp*HAL) contain an essential Tyr53-containing loop in a partially opened conformation. The modified, closed HAL structure (constructed by modeling the 39–80 loop with the catalytically essential Tyr53 on the basis of *Av*PAL) resulted in fewer deviations from the allowed side chain conformations in the Ramachandran-plot than the original experimental structure.

Investigation of distances between the acidic *pro-S* β-hydrogen at C_2 of ligand and the appropriate oxygen atoms of the possible enzymic bases Tyr53, Ty280 and Glu414 in the calculated conformations of the three proposed structures [*N*-MIO, (*R,S*)-FC, (*S,S*)-FC] of the covalently bound reaction intermediate within the closed active site of HAL revealed that the reaction can take place only via an *N*-MIO intermediate structure that allows Tyr53 to get close enough to the *pro-S* β-hydrogen. This conclusion was also supported by the docking results with (*E*)-urocanate.

DFT calculations on the role of the Zn^{2+} ion in the HAL reaction using a truncated model of the *N*-MIO intermediate indicated the formation of a tetrahedral complex with a Zn^{2+} ion coordinated to the imidazole ring of the ligand, to His83 and Met382 residues of the enzyme and to a water molecule. The formation of this transient Zn-complex could explain the narrow substrate specificity of HAL. The DFT calculations also indicated that the formation of a Zn-complex also contributed to the enhancement of the reactivity of the *pro-S* β-hydrogen in the *N*-MIO intermediate.

Acknowledgments A.L.S. is grateful for the financial support of Romanian National University Research Council (CNCSIS, PNII-TD-400). P.L. thanks the Hungarian National Science Foundation (OTKA T-048854) and the Hungarian National Office for Research and Technology (NKTH A2 2007 FLOWREAC) for financial support.

References

1. Poppe L, Rétey J (2005) Friedel-Crafts type mechanism for the enzymatic elimination of ammonia from histidine and phenylalanine. Angew Chem Int Ed 44:3668–3688. doi:10.1002/anie.200461377
2. Morrison H, Bernasconi C, Pandey G (1984) A wavelength effect on urocanic acid E/Z photoisomerization. Photochem Photobiol 40:549–550. doi:10.1111/j.1751-1097.1984.tb04632.x
3. Taylor RG, Levy HL, McInnes RR (1991) Histidase and histidinemia. Clinical and molecular considerations. Mol Biol Med 8:101–116, PMID: 1943682
4. Consevage MW, Phillips AT (1985) Presence and quantity of dehydroalanine in histidine ammonia-lyase from *Pseudomonas putida*. Biochemistry 24:301–308. doi:10.1021/bi00323a010
5. Fessenmeier M, Frank R, Schubert C, Rétey J (1991) Cloning and sequencing the urocanase gene (hutU) from *Pseudomonas putida*. FEBS Lett 286:55–57. doi:10.1016/0014-5793(91)80938-Y
6. Taylor RG, Garcia-Heras J, Sadler SJ, Lafreniere RG, Willard HF, Ledbetter DH, McInnes RR (1991) Localization of histidase to human chromosome region 12q22 → q24.1 and mouse chromosome region 10C2 → D1. Cytogenet Cell Genet 56:178–181. doi:10.1159/000133082
7. Taylor RG, Grieco D, Clarke GA, McInnes RR, Taylor BA (1993) Identification of the mutation in murine histidinemia (his) and genetic mapping of the murine histidase locus (Hal) on chromosome 10. Genomics 16:231–240. doi:10.1006/geno.1993.1164
8. Taylor RG, McInnes RR (1994) Site-directed mutagenesis of conserved serines in rat histidase. J Biol Chem 269:27473–27477, PMID: 7961661
9. Emiliani G, Fondi M, Fani R, Gribaldo S (2009) A horizontal gene transfer at the origin of phenylpropanoid metabolism: a key adaptation of plants to land. Biol Direct 4:7. doi:10.1186/1745-6150-4-7
10. Hernandez D, Phillips AT (1993) Purification and characterization of *Pseudomonas putida* histidine ammonia-lyase expressed in *Escherichia coli*. Protein Express Purif 4:473–478. doi:10.1006/prep.1993.1062
11. Taylor RG, Lambert MA, Sexsmith E, Sadler SJ, Ray PN, Mahuran DJ, McInnes RR (1990) Cloning and expression of rat histidase. Homology to two bacterial histidases and four phenylalanine ammonia-lyases. J Biol Chem 265:18192–18199, PMID: 2120224
12. Oda M, Sugishita A, Furukawa K (1988) Cloning and nucleotide sequences of histidase and regulatory genes in the *Bacillus subtilis* hut operon and positive regulation of the operon. J Bacteriol 170:3199–3205, PMID: 2454913
13. Wang L, Gamez A, Archer H, Abola EE, Sarkissian CN, Fitzpatrick P, Wendt D, Zhang J, Vellard M, Bliesath J, Bell SM, Lemontt JF, Scriver CR, Stevens RC (2008) Structural and biochemical characterization of the therapeutic *Anabaena variabilis* phenylalanine ammonia-lyase. J Mol Biol 380:623–635. doi:10.1016/j.jmb.2008.05.025
14. Calabrese JC, Jordan DB, Boodhoo A, Sariaslani S, Vanneli T (2004) Crystal structure of phenylalanine ammonia-lyase: multiple helix dipoles, implicated in catalysis. Biochemistry 43:11403–11416. doi:10.1021/bi049053+
15. Ritter H, Schulz GE (2004) Structural basis for the entrance into the phenylpropanoid metabolism catalyzed by phenylalanine ammonia-lyase. Plant Cell 16:3426–3436. doi:10.1105/tpc.104.025288
16. Schwede TF, Rétey J, Schulz GE (1999) Crystal structure of histidine ammonia-lyase revealing a novel polypeptide modification as the catalytic electrophile. Biochemistry 38:5355–5361. doi:10.1021/bi982929q
17. Poppe L (2001) Methylidene-imidazolone: a novel electrophile for substrate activation. Curr Opin Chem Biol 5:512–524. doi:10.1016/S1367-5931(00)00253-2

18. Rétey J (2003) Discovery and role of methylidene imidazolone, a highly electrophilic prosthetic group. Biochim Biophys Acta 1647:179–184. doi:10.1016/S1570-9639(03)00091-8
19. Baedeker M, Schulz GE (2002) Autocatalytic peptide cyclization during chain folding of histidine ammonia-lyase. Structure 10:61–67. doi:10.1016/S0969-2126(01)00692-X
20. Röther D, Merkel D, Rétey J (2000) Spectroscopic evidence for a 4-methylidene imidazol-5-one in histidine and phenylalanine ammonia-lyases. Angew Chem Int Ed 39:2462–2464. doi:10.1002/1521-3773(20000717)39:14<2462::AID-ANIE2462>3.0.CO;2-H
21. Wang L, Gamez A, Sarkissian CN, Straub M, Patch MG, Han GW, Striepeke S, Fitzpatrick P, Scriver CR, Stevens RC (2005) Structure-based chemical modification strategy for enzyme replacement treatment of phenylketonuria. Mol Gen Metab 86:134–140. doi:10.1016/j.ymgme.2005.05.012
22. Moffitt MC, Louie GV, Bowman ME, Pence J, Noel JP, Moore BS (2007) Discovery of two cyanobacterial phenylalanine ammonia lyases: kinetic and structural characterization. Biochemistry 46:1004–1012. doi:10.1021/bi061774g
23. Louie GV, Bowman ME, Moffitt MC, Baiga TJ, Moore BS, Noel JP (2006) Structural determinants and modulation of substrate specificity in phenylalanine-tyrosine ammonia-lyases. Chem Biol 13:1327–1338. doi:10.1016/j.chembiol.2006.11.011
24. Walker KD, Klettke K, Akiyama T, Croteau R (2004) Cloning, heterologous expression, and characterization of a phenylalanie aminomutase involved in taxol biosynthesis. J Biol Chem 279:53947–53954, PMID: 15494399
25. Steele CL, Chen Y, Dougherty BA, Li W, Hofstead S, Lam KS, Xing Z, Chiang SJ (2005) Purification, cloning, and functional expression of phenylalanine aminomutase: the first committed step in taxol side-chain biosynthesis. Arch Biochem Biophys 438:1–10. doi:10.1016/j.abb.2005.04.012
26. Mutatu W, Klettke KL, Foster C, Walker KD (2007) Unusual mechanism for an aminomutase rearrangement: Retention of configuration at the migration termini. Biochemistry 46:9785–9794. doi:10.1021/bi700691p
27. Christenson SD, Liu W, Toney MD, Shen B (2003) A novel 4-methylideneimidazole-5-one-containing tyrosien aminomutase in enediyne antitumor antibiotic C-1027 biosynthesis. J Am Chem Soc 125:6062–6063. doi:10.1021/ja034609m
28. Christianson CV, Montavon TJ, Van Lanen SG, Shen B, Bruner SD (2007) The structure of l-tyrosine 2, 3-aminomutase from the C-1027 enediyne antitumor antibiotic biosynthetic pathway. Biochemistry 46:7205–7214. doi:10.1021/bi7003685
29. Smith TA, Cordelle FH, Abeles RH (1967) Inactivation of histidine deaminase by carbonyl reagents. Arch Biochem Biophys 120:724–725. doi:10.1016/0003-9861(67)90540-1
30. Hanson KR, Havir EA (1970) L-phenylalanine ammonia-lyase. IV. Evidence that the prosthetic group contains a dehydroalanyl residue and mechanism of action1. Arch Biochem Biophys 141:1–17. doi:10.1016/0003-9861(70)90100-1
31. Hermes JD, Weiss PM, Cleland WW (1985) Use of nitrogen-15 and deuterium isotope effects to determine the chemical mechanism of phenylalanine ammonia-lyase. Biochemistry 24:2959–2967. doi:10.1021/bi00333a023
32. Langer M, Pauling A, Rétey J (1995) The role of dehydroalanine in catalysis by histidine ammonia-lyase. Angew Chem Int Ed 34:1464–1465. doi:10.1002/anie.199514641
33. Röther D, Poppe L, Viergutz S, Langer B, Rétey J (2001) Characterization of the active site of histidine ammonia-lyase from *Pseudomonas putida*. Eur J Biochem 268:6011–6019. doi:10.1046/j.0014-2956.2001.02298.x
34. Röther D, Poppe L, Morlock G, Viergutz S, Rétey J (2002) An active site homology model of phenylalanine ammonia-lyase from *Petroselinum crispum*. Eur J Biochem 269:3065–3075. doi:10.1046/j.1432-1033.2002.02984.x
35. Klee CB (1972) Metal activation of histidine ammonia-lyase. Metal ion-sulfhydryl group relationship. J Biol Chem 247:1398–1406, PMID: 4622230
36. Givot IL, Smith TA, Abeles RA (1969) Studies on the mechanism of action and the structure of the electrophilic center of histidine ammonia lyase. J Biol Chem 244:6341–6353, PMID: 5354960
37. Baedeker M, Schulz GE (2002) Structures of two histidine ammonia-lyase modifications and implications for the catalytic mechanism. Eur J Biochem 269:1790–1797. doi:10.1046/j.1432-1327.2002.02827.x
38. Seff AL, Pilbák S, Poppe L (2008) Ligand docking and systematic conformational analysis in loop modified parsley phenylalanine ammonia-lyase structure. Studia Universitatis Babes-Bolyai Chemia, LIII 53(2):67–71, ISSN 1224-7154
39. Bartsch S, Bornschauer UT (2009) A single residue influences the reaction mechanism of ammonia lyases and mutases. Angew Chem Int Ed 48:3362–3365. doi:10.1002/anie.200900337
40. Swiss-PDBViewer version 4.0 (http://www.expasy.org/spdbv/)
41. Guex N, Peitsch MC (1997) SWISS-MODEL and the Swiss-Pdb viewer: an environment for comparative protein modeling. Electrophoresis 18:2714–2723. doi:10.1002/elps.1150181505
42. Schwede T, Kopp J, Guex N, Peitsch MC (2003) SWISS-MODEL: an automated protein homology-modeling server. Nucleic Acid Res 31:3381–3385. doi:10.1093/nar/gkg520
43. SWISS-MODEL (http://swissmodel.expasy.org/).
44. Arnold K, Bordoli L, Kopp J, Schwede T (2006) The SWISS-MODEL workspace: a web-based environment for protein structure homology modelling. Bioinformatics 22:195–201. doi:10.1093/bioinformatics/bti770
45. Kopp J, Schwede T (2004) The SWISS-MODEL repository of annotated three-dimensional protein structure homology models. Nucleic Acids Res 32:D230–D234. doi:10.1093/nar/gkh008
46. Peitsch MC (1995) Protein modelling by e-mail. Bio/Technology 13:658–660. doi:10.1038/nbt0795-658
47. HyperChem version 7.0 (Hypercube, Inc. http://www.hyper.com/)
48. Molfunction, Institute of Molecular Function (http://www.molfunction.com/)
49. Morris GM, Goodsell DS, Halliday RS, Huey R, Hart WE, Belew RK, Olson AJ (1998) Automated docking using a Lamarckian genetic algorithm and an empirical binding free energy function. J Comput Chem 19:1639–1662. doi:10.1002/(SICI)1096-987X(19981115)19:14<1639:AID-JCC10>3.0.CO;2-B
50. Huey R, Morris GM, Olson AJ, Goodsell DS (2007) A semiempirical free energy force field with charge-based desolvation. J Comput Chem 28:1145–1152. doi:10.1002/jcc.20634
51. Frisch MJ, Trucks GW, Schlegel HB, Scuseria GE, Robb MA, Cheeseman JR, Scalmani G, Barone V, Mennucci B, Petersson GA, Nakatsuji H, Caricato M, Li X, Hratchian HP, Izmaylov AF, Bloino J, Zheng G, Sonnenberg JL, Hada M, Ehara M, Toyota K, Fukuda R, Hasegawa J, Ishida M, Nakajima T, Honda Y, Kitao O, Nakai H, Vreven T, Montgomery JA Jr, Peralta JE, Ogliaro F, Bearpark M, Heyd JJ, Brothers E, Kudin KN, Staroverov VN, Kobayashi R, Normand J, Raghavachari K, Rendell A, Burant JC, Iyengar SS, Tomasi J, Cossi M, Rega N, Millam NJ, Klene M, Knox JE, Cross JB, Bakken V, Adamo C, Jaramillo J, Gomperts R, Stratmann RE, Yazyev O, Austin AJ, Cammi R, Pomelli C, Ochterski JW, Martin RL, Morokuma K, Zakrzewski VG, Voth GA, Salvador P, Dannenberg JJ, Dapprich S, Daniels AD, Farkas O, Foresman JB, Ortiz JV, Cioslowski J, Fox DJ (2009) Gaussian 09, Revision A.1. Gaussian Inc, Wallingford
52. Dennington R II, Keith T, Millam J, Eppinnett K, Hovell WL Gilliland R (2003) GaussView, Version 3.09. Semichem Inc, Shawnee Mission
53. Becke AD (1993) Density-functional thermochemistry. III. The role of exact exchange. J Chem Phys 98:5648–5652. doi:10.1063/1.464913

54. Lee C, Yang W, Parr RG (1988) Development of the Colle-Salvetti correlation-energy formula into a functional of the electron density. Phys Rev B 37:785–789. doi:10.1103/PhysRevB.37.785
55. Pilbák S, Tomin A, Rétey J, Poppe L (2006) The essential tyrosine-containing loop conformation and the role of the C-terminal multi-helix region in eukaryotic phenylalanine ammonia-lyases. FEBS J 273:1004–1019. doi:10.1111/j.1742-4658.2006.05127.x
56. Klee CB (1974) Stereospecific irreversible inhibition of histidine ammonia-lyase by L-cysteine. Biochemistry 13:4501–4507. doi:10.1021/bi00719a005
57. Hernandez D, Stroh JG, Phillips AT (1993) Identification of Ser^{143} as the site of modification in the active site of histidine ammonia-lyase. Arch Biochem Biophys 307:126–132. doi:10.1006/abbi.1993.1570
58. Merkel D, Rétey J (2000) Further insight into the mechanism of the irreversible inhibition of histidine ammonia-lyase by L-cysteine and dioxygen. Helv Chim Acta 83:1151–1160. doi:10.1002/1522-2675(20000607)83:6<1151::AID-HLCA1151>3.0.CO;2-4
59. Galpin JD, Ellis BE, Tanner ME (1999) The inactivation of histidine ammonia-lyase by L-cysteine and oxygen: modification of the electrophilic center. J Am Chem Soc 121:10840–10841. doi:10.1021/ja992729h
60. Peterkofsky A (1962) The mechanism of action of histidase: amino-enzyme formation and partial reactions. J Biol Chem 237:787–795, PMID: 14485719
61. Christianson CV, Montavon TJ, Festin GM, Cooke HA, Shen B, Bruner SD (2007) The mechanism of MIO-based aminomutases in β-amino acid biosynthesis. J Am Chem Soc 129:15744–15745. doi:10.1021/ja0762689
62. Montavon TJ, Christianson CV, Festin GM, Shen B, Bruner SD (2008) Design and characterization of mechanism-based inhibitors for the tyrosine aminomutase SgTAM. Bioorg Med Chem Lett 18:3099–3102. doi:10.1016/j.bmcl.2007.11.046
63. Schroeder AC, Kumaran S, Hicks LM, Cahoon RE, Halls C, Yu O, Jez JM (2008) Contribution of conserved serine and tyrosine residues to catalysis, ligand binding, and cofactor processing in the active site of tyrosine ammonia lyase. Phytochemistry 69:1496–1506. doi:10.1016/j.phytochem.2008.02.007
64. Hanson KR (1981) Phenylalanine ammonia-lyase: mirror image packing of D- and L-phenylalanine and D- and L-transition state analogs into the active site. Arch Biochem Biophys 211:575–588. doi:10.1016/0003-9861(81)90492-6
65. Meldrum NU, Roughton FJ (1933) Carbonic anhydrase. Its preparation and properties. J Physiol 80:113–142, PMID: 16994489
66. Berg JM, Tymoczko JL, Stryer L (2002) Biochemistry, 5th edn. Freeman, New York
67. Glusker JP (1991) Structural aspects of metal liganding to functional groups in proteins. Adv Protein Chem 42:1–76, PMID: 1793004
68. Rulísek L, Vondrásek J (1998) Coordination geometries of selected transition metal ions (Co^{2+}, Ni^{2+}, Cu^{2+}, Zn^{2+}, Cd^{2+}, and Hg^{2+}) in metalloproteins. J Inorg Biochem 71:115–127. doi:10.1016/S0162-0134(98)10042-9
69. Zheng H, Chruszcz M, Lasota P, Lebioda L, Mino W (2008) Data mining of metal ion environments present in protein structures. J Inorg Biochem 102:1765–1776. doi:10.1016/j.jinorgbio.2008.05.006
70. Nauton L, Kahn R, Garau G, Hernandez JF, Dideberg O (2008) Structural insights into the design of inhibitors for the L1 metallo-β-lactamase from *Stenotrophomonas maltophilia*. J Mol Biol 375:257–269. doi:10.1016/j.jmb.2007.10.036
71. Lipscomb WS, Strater N (1996) Recent advances in zinc enzymology. Chem Rev 96:2375–2433. doi:10.1021/cr950042j
72. Gerhardt S, Hassal G, Hawtin P, McCall E, Flavell E, Minshull C, Hargreaves D, Ting A, Pauptit RA, Parker AE, Abbott WM (2007) Crystal structures of human ADAMTS-1 reveal a conserved catalytic domain and a disintegrin-like domain with a fold homologouse to cysteine-rich domains. J Mol Biol 373:891–902. doi:10.1016/j.jmb.2007.07.047
73. Bebrone C (2007) Metallo-β-lactamases (classification, activity, genetic organization, structure, zinc coordination) and their superfamily. Biochem Pharmacol 74:1686–1701. doi:10.1016/j.bcp.2007.05.021
74. Debela M, Goettic P, Magdolen V, Huber R, Schechter NM, Bode W (2007) Structural basis of the zinc inhibition of human tissue Kallikrein 5. J Mol Biol 373:1017–1031. doi:10.1016/j.jmb.2007.08.042
75. Klee CB, Kirk KL, Cohen LA, McPhie P (1975) Histidine ammonia-lyase. The use of 4-fluorohistidine in identification of the rate determining step. J Biol Chem 250:5033–5040, PMID: 1150653
76. Klee CB, Kirk KL, Cohen LA (1979) 4-Nitro-L-histidine as a substrate for histidine ammonia-lyase: the role of beta-hydrogen acidity in the rate-limiting step. Biochem Biophys Res Commun 87:343–348, PMID: 36890
77. Gomis-Rüth FX, Kress LF, Bode W (1993) First structure of a snake venom metalloproteinase: a prototype for matrix metalloproteinases/collagenases. EMBO J 12:4151–4157, PMID: 8223430